An Examination of School Reopening Strategies during the SARS-CoV-2 Pandemic

Alfonso Landeros[1], Xiang Ji[2], Kenneth Lange[1,3], Timothy C. Stutz[1], Jason Xu[4], Mary E. Sehl[*,1,5], Janet S. Sinsheimer[*,1,3,6]

[1]Department of Computational Medicine, David Geffen School of Medicine at UCLA, USA
[2]Department of Mathematics, School of Science & Engineering, Tulane University, USA
[3]Department of Human Genetics, David Geffen School of Medicine at UCLA, USA
[4]Department of Statistical Science, Duke University, USA
[5]Division of Hematology-Oncology, Department of Medicine, David Geffen School of Medicine at UCLA, USA
[6]Department of Biostatistics, UCLA Fielding School of Public Health, USA

August 5, 2020

Abstract

The SARS-CoV-2 pandemic led to the closure of nearly all K-12 schools in the United States of America in March 2020. Although reopening K-12 schools for in-person schooling is desirable for many reasons, officials also understand that risk reduction strategies and detection of cases must be in place to allow children to safely return to school. Furthermore, the consequences of reclosing recently reopened schools are substantial and impact teachers, parents, and ultimately the educational experience in children. Using a stratified Susceptible-Exposed-Infected-Removed model, we explore the influences of reduced class density, transmission mitigation (such as the use of masks, desk shields, frequent surface cleaning, or outdoor instruction), and viral detection on cumulative prevalence. Our model predicts that a combination of all three approaches will substantially reduce SARS-CoV-2 prevalence. The model also shows that reduction of class density and the implementation of rapid viral testing, even with imperfect detection, have greater impact than moderate measures for transmission mitigation.

Introduction

The best way to reopen K-12 schools has justifiably been a topic of intense discussion among government officials, the media, teachers and parents. Given transmission of SARS-CoV-2 occurs through respiratory droplets, any reopening policy must adequately reduce crowded environments at school to protect children, teachers, staff, and ultimately communities. Unfortunately, many factors work to the detriment of ostensibly reasonable strategies. For example, splitting a school day into morning and afternoon blocks may extend teachers' working hours or fail to adequately reduce class density in already overcrowded school districts. Primary caretakers who work outside the home face additional challenges in dropping off and picking up children from school. Finally, there is the issue of the quality of educational experiences to consider. A recent study on the effects of school closure in March in the U.S. suggests that it reduced COVID-19 cases in states with low cumulative incidence [2], yet education researchers worry that teachers will face lagging educational development of children once schools reopen due to the extended period of remote learning [11]. A

predictable, regular attendance policy is crucial in balancing social burden with maintaining steady educational progress.

Having to close schools that have reopened due to an unacceptable risk in COVID-19 cases is a serious concern and has prompted the inclusion of stopping rules in guidelines for school reopening [31]. As school systems have proposed different scenarios of reopening to reduce the density of students and the number of student interactions, it is helpful to investigate quantitatively the ramifications of the proposed plans. Here we explore a simple and interpretable mathematical model that compares the infection rates in children and adults under various reopening scenarios. Our approach stratifies members of a school community into two age groups, school-age children and adults, and assigns children to a single or two or three different cohorts. The two age groups differ in size, but within each group all children or all adults exhibit homogeneous disease behavior. With multiple cohorts, the goal is to limit the density of children in the classroom at a given time. Specifically, we compare the consequences of (1) reopening at full capacity, (2) allowing half of all children to return to in-person schooling while the other half continues with remote learning (parallel cohorts) and (3) alternating sessions in which different cohorts of students attend school by the week (rotating cohorts). The latter scenario is designed to reduce classroom density and contacts between children while providing some of the benefits of in-person learning to all children. Our goal is to provide insight into the epidemiological implications of these reopening strategies and to quantify their consequences. In particular, we explore implications of the recent guidelines announced by Governor Gavin Newsom for California schools [31].

We find that reopening schools at half capacity, by running either two parallel cohorts of in-person and remote learning or two rotating cohorts of in-person learning, is likely to have a greater impact in controlling virus spread than direct measures that mitigate transmission risk. That is, reducing the number or density of contacts produces a larger effect than diminishing the transmission rate per contact. Our models also suggest that the regular administration of rapid surveillance tests, even with imperfect sensitivity, can significantly delay disease outbreaks. It is our hope that our results along with further data and modeling by other experts will guide public health policy decisions.

Methods

Compartmental model. Our approach uses a deterministic Susceptible-Exposed-Infected-Removed (SEIR) model stratified by age group and cohort. In full generality, let $S(t)$, $E(t)$, $I(t)$, and $R(t)$ denote the fraction of susceptible, exposed, infected, and removed individuals, respectively, in the overall population at time t. Infecteds may or may not present with symptoms. The removed pool accounts for individuals with negligible contribution to the spread of infection, including individuals that have either recovered with full immunity or are no longer part of the population due to disabling morbidity or death. Although prospects that infection leads to permanent immunity are unclear, immunity on the time scale of several months or more is plausible [20], so we make the assumption that individuals do not return to the susceptible pool once they are infected.

Denote by $I_{il}(t)$ the fraction of infecteds in age group i and cohort l. We propose the following frequency-dependent model for the force of infection on individuals in age group j and cohort k:

$$\begin{array}{c}\text{force of}\\ \text{infection}\end{array} = \begin{pmatrix}\text{interaction}\\ \text{between}\\ \text{cohorts } k,\ell\end{pmatrix} \times \begin{pmatrix}\text{transmission}\\ \text{between age}\\ \text{groups } i \to j\end{pmatrix} \times \begin{pmatrix}\text{fraction of}\\ \text{infecteds in}\\ \text{age group } i,\\ \text{and cohort } \ell\end{pmatrix}$$

$$\lambda_{jk}(t) = \sum_{\ell}\sum_{i} \alpha_{k\ell} \times \beta_{ij}(t) \times I_{i\ell}(t)$$

For pairs of cohorts $k \neq \ell$, the choice $\alpha_{kl} = 0$ reflects complete separation, whereas $\alpha_{kl} = 1$ corresponds to complete mixing under no mitigating policies. Values in between these limits may be interpreted as decreased interaction due to physical or social distancing. We allow for weak cohort interaction ($\alpha_{k\ell} = 0.05$, $k \neq \ell$) in all our simulations. To capture the variability in exposure to infectious individuals across age groups and different cohorts, the transmission rate $\beta_{ij}(t)$ is time-inhomogeneous. These choices effectively model the density dependence of coronavirus transmission on cohort isolation and contact patterns between different age groups.

We model two age groups, children and adults, and ignore vital dynamics (that is, ordinary births and deaths) altogether. The latter choice is justified by the relatively short time period over which the model acts. The resulting ordinary differential equation (ODE) subsystem describing cohort k is given by

$$\begin{aligned}
\frac{\mathrm{d}S_{1k}}{\mathrm{d}t} &= -\lambda_{1k} S_{1k} & \frac{\mathrm{d}S_{2k}}{\mathrm{d}t} &= -\lambda_{2k} S_{2k} \\
\frac{\mathrm{d}E_{1k}}{\mathrm{d}t} &= \lambda_{1k} S_{1k} - \sigma_1 E_{1k} & \frac{\mathrm{d}E_{2k}}{\mathrm{d}t} &= \lambda_{2k} S_{2k} - \sigma_2 E_{2k} \\
\frac{\mathrm{d}I_{1k}}{\mathrm{d}t} &= \sigma_1 E_{1k} - \gamma_1 I_{1k} & \frac{\mathrm{d}I_{2k}}{\mathrm{d}t} &= \sigma_2 E_{2k} - \gamma_2 I_{2k} \\
\frac{\mathrm{d}R_{1k}}{\mathrm{d}t} &= \gamma_1 I_{1k} & \frac{\mathrm{d}R_{2k}}{\mathrm{d}t} &= \gamma_2 I_{2k},
\end{aligned}$$

with the left and right columns corresponding to children and adults, respectively. For simplicity in communicating the key ideas in our model, we limit the scope of simulations to two age groups, children in K-12 education and individuals over the age of 18, and to 1 to 3 child cohorts. We also neglect any inhomogeneity in susceptibility and transmission within each of the two age groups [4, 9]. To our credit, we emphasize the interplay of transmission across and within age classes, that is the ratios β_{ii}/β_{jj} and β_{ij}/β_{ji}. By design, our model makes it easy to explicitly incorporate susceptibility, contact patterns, and, ultimately, finer age stratification. In broad outline, our model is similar to that of Zhang et al. [26]. However, these researchers emphasize differences in contact patterns across age groups rather than school reopening policies.

Cohort structure and transmission rates. Previous work suggests that a cyclic attendance strategy tuned to the latent period of SARS-CoV-2 may curtail secondary infections [10]. To compare with full-time and online-only instruction, we investigate the consequences of reopening at 50% and 33% capacity with rotating cohorts. Assuming a latent period within the range of 3–4 days, a weekly rotation schedule synchronizes with peak infectiousness. Our simulations therefore model transmission between children using periodic rates that cycle between high and low contact values. Namely, we take $\beta_{11}(t) = c \times \beta$ on school days and $\beta_{11}(t) = \beta$ otherwise, where β is a baseline rate outside of school and c is a multiplier increasing transmission between children. This function is phased between cohorts to reflect school rotation. In summary, children in rotating cohorts attend school for 5 consecutive days and then rotate with the next cohort at the beginning of the following week. With two cohorts children attend school every other week; for three cohorts they attend every third week. As noted previously, this is referred to as the rotating cohort strategy. An emerging national trend in the U.S. is to allow families to opt for remote learning in lieu of in-person instruction during the SARS-CoV-2 pandemic. Specifically, we divide our virtual school community into two cohorts of equal size, one of which attends school and thus has the elevated transmission rate while a second group opts for a remote learning option. This is referred to as the parallel cohort strategy.

Choice of model parameters. As of August 3, 2020, the CDC reports 4.6 million COVID-19 cases in the United States [32]. California, Florida, and Texas are each burdened with nearly 0.5 million cases, which corresponds to 1% infection in their respective populations. Given that the U.S. has considerable variation in density, we seed all our simulations, which represent school communities rather than states, with 0.1% infected individuals. Increasing this value accelerates infections in our model; decreasing it lessens the spread. Our simulations therefore represent scenarios far from herd immunity [12, 21].

Although children have fewer symptoms, less severe disease, and lower case-fatality rates than adults, they may be just as prone to SARS-CoV-2 infections as adults [28]. Children may present with a variety of symptoms ranging from fever, rhinitis, cough, and GI symptoms, to a Kawasaki-like disease [22]. However, because children's symptoms are typically less severe and of shorter duration than those of adults, the likelihood of pediatric infection escaping symptom-based monitoring, such as temperature screening, is therefore is higher than that of adults and increases asymptomatic transmission. Thus, detecting transmission between children specifically is difficult; quantifying it is all the more challenging. An analysis of contact tracing data from Singapore suggests that per contact transmission between children, particularly in educational settings, is low compared to adult-adult transmission [24]. Yet the number of contacts between children is expected to be significantly higher compared to other age groups [26]. Li et al. provide estimates for transmission rates in Wuhan prior to (1.12 per day) and following travel restrictions (0.52 per day) [16]. Reconciling estimates of transmission rates across populations, which are necessarily based on different scientific models, is unproductive in proposing policy. Instead, we vary each β_{ij} in simulations to underscore the influence of modeling assumptions on epidemiological consequences. In later simulations we opt to model child-to-child transmission with lower rates to reflect evidence suggesting children are rarely index cases [15] and have fewer contacts outside of school. In this setting, transmission is elevated by a factor c in children only on school days, $\beta_{11}(t) = c \times \beta$, so as to account for increased contacts. A recent study indicates that viral RNA in the nasopharynx of young children is elevated compared to adults [8], partially justifying this modeling choice.

In contrast to contact rates, the latent, infectious, and incubation periods for SARS-CoV-2 are well characterized in the literature. Lauer et al. estimate a median incubation period of approximately 5 days [14]. Li et al. [16] infer latency and infectious periods of 3.69 and 3.47 days, respectively, in a study aimed at characterizing contributions of undocumented infections to disease spread in China. The review by Bar-On draws from these studies and reports median latent and infectious periods of 3 and 4 days, respectively [3]. Other studies report serial intervals and incubation periods consistent with these estimates for latency and infectiousness [6, 7]. Unfortunately, the literature on similar epidemiological inferences in children is sparse. Table 1 summarizes our choices and lists references pertinent to each choice.

Basic reproductive number. We now characterize the basic reproductive number $\mathcal{R}_0$ indicative of the growth potential of an epidemic. Specifically, $\mathcal{R}_0$ quantifies the expected number of secondary infections due to a single infected within a completely susceptible population. The threshold $\mathcal{R}_0$ value of 1 marks the boundary between explosive growth ($\mathcal{R}_0 > 1$) and decline of an epidemic to extinction ($\mathcal{R}_0 < 1$). We characterize $\mathcal{R}_0$ using the next generation method as outlined by Diekmann, Heesterbeek, and Roberts [5]. Under the assumption that viral infections have been sufficiently contained in the community prior to reopening, it is reasonable to linearize dynamics by taking $S(0) \approx 1$. Thus, the transmission and transition operators $\boldsymbol{T}$ and $\boldsymbol{\Sigma}$ are given respectively

by the matrices

$$\boldsymbol{T} = \begin{bmatrix} 0 & \alpha_{11}\beta_{11}S_{11} & 0 & \alpha_{11}\beta_{21}S_{11} \\ 0 & 0 & 0 & 0 \\ 0 & \alpha_{11}\beta_{12}S_{21} & 0 & \alpha_{11}\beta_{22}S_{21} \\ 0 & 0 & 0 & 0 \end{bmatrix}, \qquad \boldsymbol{\Sigma} = \begin{bmatrix} -\sigma_1 & 0 & 0 & 0 \\ \sigma_1 & -\gamma_1 & 0 & 0 \\ 0 & 0 & -\sigma_2 & 0 \\ 0 & 0 & \sigma_2 & -\gamma_2 \end{bmatrix}$$

based on an infectious subsystem defined by $\boldsymbol{x} = [E_1, I_1, E_2, I_2]^\top$ for a single cohort, where 1 denotes children and 2 denotes adults. Together, these linear operators define an embedded subsystem that completely characterizes infectious dynamics, namely $\frac{\mathrm{d}\boldsymbol{x}}{\mathrm{d}t} = (\boldsymbol{T} + \boldsymbol{\Sigma})\boldsymbol{x}$. The standard theory identifies $\mathcal{R}_0$ as the spectral radius of $-\boldsymbol{T}\boldsymbol{\Sigma}^{-1}$, a quantity that can be computed numerically in practice. In the case of multiple cohorts, the structures of $\boldsymbol{T}$ and $\boldsymbol{\Sigma}$ as given are repeated in a tiled fashion, with the appropriate changes in indices for $\alpha_{k\ell}$ and $S_{j\ell}$.

Results

Effect of reducing density via cohorts. Transmission of SARS-CoV-2 is thought to occur primarily through respiratory droplets. Thus, it is critical to first examine the effect of separating children into several rotating cohorts in our model, which implicitly reduces density via the contact network of a population. Figure 1 summarizes the influence of time-homogeneous transmission rates $\beta_{ij}(t) = \beta_{ij}$ on the reproductive number $\mathcal{R}_0$ under various scenarios, assuming a population mix of 55% children and 45% adults and strong adherence to mitigation policies (with $\alpha_{k\ell} = 0.05$ for each $k \neq \ell$) that keep both children and adults isolated from members of other cohorts. Splitting a school community into even 2 or 3 rotating cohorts substantially reduces $\mathcal{R}_0$ under a wide range of parameter values and slows viral spread in cases of moderate transmissibility. For example, moving from full capacity to 2 cohorts reduces $\mathcal{R}_0$ by 50% for the range $0 \leq \beta_{11}, \beta_{22} \leq 1$ (Figure 1, A and 1B). Using three cohorts further reduces $\mathcal{R}_0$ for comparable β_{11} and β_{22} (Figure 1C). This parameter range is of interest because it corresponds to $\mathcal{R}_0 \approx 2$ in the full capacity scenario. Likewise, two or three rotating cohorts for children also decrease $\mathcal{R}_0$ when transmission rates between children and adults are asymmetric; that is, $\beta_{12} > \beta_{21}$ or $\beta_{12} < \beta_{21}$ (Figure 1, D to F). As demonstrated by the skew present in our contour plots, age structure amplifies the influence of transmission rates.

Reopening under stopping rules. We now consider the effect of a stopping rule on cumulative prevalence. Inspired by California's recent guidelines that urge schools to close down whenever the percent of infecteds within a school reaches 5% over a 2 week period [31], we use a cumulative prevalence of 5% as a stopping rule. In symbols, the stopping rule is given by the condition

$$\text{sensitivity} \times \sum_k [I_{1,k}(t) + R_{1,k}(t)] \geq 5\%,$$

which relies on the detection of cases on school days as well as on surveillance reports from outside of school. Detection is based on testing at the beginning of a school day, after which infected individuals in the active cohort are immediately isolated and placed in the removed state ($I(t) \to R(t)$). The isolation rule does not apply to the out of school cohort or cohorts. The sensitivity factor in the rule captures imprecision in testing and reporting. Because our model does not explicitly account for adult staff at school, we measure only the cumulative prevalence within the child population. This choice is partially justified because students typically well outnumber teachers and ancillary staff. Under the assumption of a 20:1 student-staff ratio, a school with 1000 students would need approximately 53 cases in a 14-day period to meet the closure criterion. Please note

that our simulations deviate from California's proposed policy by tracking cumulative cases rather than cases within a sliding 14-day window.

Figure 2 reports the number of weeks to reach the 5% threshold in our model in various parameter regimes, assuming the monitoring program exactly identifies infections in children as they begin a new day of school. Cohort separation tends to dramatically reduce the spread of infection. Owing to high child-to-child transmission effects within school ($c = 10$), our model predicts closures within a month in a full-capacity high transmission scenario with no mitigation (Figure 2, A and E). Under the more optimistic assumption of preventive measures, hitting the 5% threshold may take several weeks and may, in fact, never occur in the ideal circumstances of low density and effective risk mitigation (Figure 2, B to D and F to H). Notably, under most of the parameter values we chose, 2 parallel cohorts and 2 rotating cohorts show similar time to 5% infecteds, with the parallel cohort strategy having a slight advantage when β_{11} and β_{22} are large. For example when $\beta_{11} = 1$ and $\beta_{22} = 1$, 2 rotating cohorts reach the 5% infected level in 6 to 8 weeks, and 2 parallel cohorts reach it in 8 to 10 weeks (Figure 2, B and C). This behavior is partially driven by the testing protocol, which only detects and isolates cases in the active cohort.

Unfortunately, the issue of detection is complicated by the availability of testing resources, administration of tests, and specificity of the tests used. In light of this reality, we compare predictions of our model over 6 months when (1) no action is taken (Figure 3, A and B), (2) the monitoring program uses a perfectly sensitive test with no delays in reporting (Figure 3, C and D), and (3) the monitoring program uses a rapid but less sensitive test (Figure 3, E and F). Our simulations with a single cohort indicate that a 5% percent threshold policy can shift infections in children from 80% to 55% over a 6 month period when child-to-child transmission rates in school are high (Figure 3C). Compared to this ideal testing scenario, an imperfect test with 50% detection leads to an earlier stopping time, owing to infections spread by undetected cases, and to greater pediatric infections but still far less than the no testing scenario (Figure 3E). Let us emphasize our finding that reopening with a surveillance program in place may provide 10 to 12 weeks of continuous instruction with low infection risk. Infections after closing are driven by a lack of interventions outside of school; testing and isolation in this context can curtail this growth. In general, our results support the importance of testing and the failsafe of complete school closure in preventing a major disease outbreak after reopening.

Next, we explore the ramifications of two parallel cohorts using the simulation study design just considered. Specifically, we assume the elevated transmission rate $\beta_{11}(t) = c \times 0.15$ during a regular 5-day school week and and the reduced transmission rate $\beta_{11}(t) = 0.15$ during the off week. The remaining transmission rates are chosen with $\mathcal{R}_0 > 1$ to capture outbreak conditions. These choices lead to more rapid acting infection and earlier school closure than those chosen in Figure 3 under the single cohort policy. Figure 4 reports the same indices recorded in our simulation study with the single cohort policy. As our earlier figures illustrate, reducing density through the community's contact network successfully decreases cumulative prevalences, sustained contact between children notwithstanding (Figure 4, A to D). The in-person stopping rule (the entire school goes online when cumulative prevalence reaches 5%) is triggered even when detection is imperfect (Figure 4, E to F). Because cohorts reduce contacts, our model predicts a longer period of instruction (18-22 weeks) with the parallel strategy (Figure 4, C and E) compared to the previous simulation with all students attending at once (10-12 weeks) (Figure 3, C and E). We note that, despite the remote cohort child-to-child transmission rate being 1/10 of the in-person cohort child-to-child rate, the remote cohort has more infections than the in-person cohort in both surveillance scenarios. This result occurs because only the latter cohort is monitored through the school's testing program. One may interpret this as an upper bound on infections for the remote learning cohort as there will likely be some monitoring for this group in practice.

Mitigating transmission between children. Transmission mitigation strategies that may work well for adults may be less practical to implement with children. As an example, although face masks have been shown to reduce the spread of SARS-CoV-2 by 40% [17], there are valid concerns about the ill effects of mask wearing by elementary school children. These concerns include impaired learning, speech development, social development, and facial recognition [29]. There is also doubt about whether young children can properly keep their masks on. The protection gained from mask wearing needs to be weighed against the disadvantages just enumerated. Regardless of their form, we assume that effective strategies will be employed. Using reasonable approximations for contact and transmission risks, we explore the impacts of varying degrees of protection conferred by combined risk reduction strategies, including but not limited to mask wearing, desk shields, hand washing, vigilant cleaning of surfaces, improved ventilation, and outdoor instruction. The combined impacts of these risk reduction strategies are modeled as 20%, 40%, 60%, and 80% reductions in the transmission rates β_{11} and β_{12} relative to reference values. We particularly examine the changes in infection levels under each scenario, taking care in selecting the adult values β_{21} and β_{22} to account for simultaneous risk reduction strategies among adults. Specifically, we take $\beta_{11} = 0.1$ and $\beta_{12} = \beta_{21} = \beta_{22} = 0.5$ as natural rates. Under a baseline model reducing transmission rates in adults to $\beta_{21} = \beta_{22} = 0.2$, we achieve an $\mathcal{R}_0 \approx 1.8$ when schools remain closed. We choose to model increased contact rates $\beta_{11}(t) = c \times 0.1$ by taking $c = 10$, which corresponds to $\mathcal{R}_0 \approx 3.3$ under the full capacity reopening scenario. This necessarily represents an extreme that illustrate effects in a poor situation.

Figure 5 compares prevalence trajectories by interventions directly targeting transmission under a single or two rotating child cohorts. With a single cohort and no mitigation, our choices lead to approximately 2%, 46%, and 65% infected children after 1, 3, and 6 months following reopening, respectively (Figure 5A). However, with measures that lead to an 80% reduction in transmission, it would take more than 24 weeks to reach a cumulative prevalence of 5% in children (Figure 5A). Achieving an 80% reduction in transmission would be difficult in practice. With a more realistic reduction factor of only 20%, our model predicts that 5% cumulative prevalence in children would be reached in roughly 8 weeks (Figure 5A). Targeting transmission rates in children also reduces infections in adults to a similar degree (Figure 5B). Although policies such as mask use and hand washing have an appreciable effect in reducing infections, our model predicts the intuitive conclusion that stricter adherence to transmission mitigation measures is required to lead to low levels of infection when there is a single cohort than when there are two cohorts. In fact, we show that an 80% reduction in child-to-child transmission is required to lead to 0.5% pediatric infections over 6 months, which is roughly equivalent to the effect of 2 rotating cohorts (Figure 5C, D) without mitigation strategies. A combination of both types of interventions ultimately results in even fewer infections.

Discussion

Our models highlight the profound potential impact of reducing cohort size with parallel or rotating cohorts under a range of transmission rates and reproduction numbers. For example, if we take transmission rates $\beta_{11} = \beta_{22} = 1$, it would take approximately 2 weeks to reach a threshold of 5% children infected, whereas under the same transmission rates splitting the school population into two or three rotating cohorts would lead to a month or more of uninterrupted instruction (Figure 2). Quite apart from cohort strategies, our work also reveals the importance of tracking infections and setting a threshold for reverting to remote learning. In the absence of any intervention to in-person instruction, the cumulative proportion of the school children population can quickly reach 20% within 6 weeks (Figure 3A). This compares with keeping that cumulative proportion at $5 - 10\%$

for at least 3 months under the combination of a rapid testing program, a stopping rule, and just a single cohort (Figure 3C). Finally, our results demonstrate that simultaneous adherence to transmission mitigation measures and multiple separated cohorts can keep cases low, for example under 0.5% (Figure 5C,D).

There are several limitations to our simulations. First, we account only for two separate age classes, children and adults. A finer level of age stratification may be better suited for predicting outcomes in specific communities and is, in principle, straightforward to implement within our modeling framework. For example, our model currently makes no distinction between high school and elementary school children. High school students may be more easily convinced into wearing masks reliably and practicing physical distancing, but they also may have transmission rates closer to those of adults. Second, we treat all adults, including teachers, as having the same transmission rates and omit interactions between students and teachers within a classroom. The latter are clearly critical in implementing backup protocols that allow the switch to remote learning. A network-based model that accounts for households and classrooms in more detail would be better equipped to identify optimal policies. Third, our model treats school communities in isolation. Schools in urban settings undoubtedly have more diverse commuting patterns and face a greater potential for importing cases from outside adjacent neighborhoods. Finally, our models are deterministic and cannot account for the stochastic nature of infections. The caveats outlined here limit the quantitative accuracy of our predictions, but we contend that our qualitative conclusions are correct.

As already mentioned, our simulations suggest that measures that reduce class density by rotating cohorts between in-person and online schooling are likely to have the greatest impact in reducing the spread of SARS-CoV-2 brought on by the resumption of in-person instruction. From the perspective of mathematical epidemiology, this is to be expected as separating a contact graph into disconnected pieces ultimately limits the proliferative potential of an infectious disease. Parallel cohorts present an attractive alternative to rotating cohorts because the latter require a great deal of coordination and place a burden on parents to adjust their work schedules to match their children's in-class and at home schedules. Although less than ideal from an educational perspective, educating children under either cohort strategy should be a priority in school reopenings. Even so, our findings indicate that implementation of specific in-class policies such as mask wearing, hand washing, and physical distancing in the classroom will be helpful in reducing transmission rates. Our simulations of a backup plan to switch to remote learning when the number of infections climbs to an unacceptable level emphasize the need for rapid testing and efficacious surveillance programs. These results are consistent with a recent study on the influence of viral kinetics, test sensitivity, test frequency, and sample-to-answer reporting time in surveillance protocols [13]. This study concludes that test efficacy should be a secondary concern in implementing testing given the dangers of the current pandemic.

Finally, different communities should be treated differently. High-risk communities with large class sizes need to be especially careful in exposing children to unnecessary risks. We are happy to share our software and assist in its improvement. Until effective vaccines become available, we are in a battle against time in limiting mortality and morbidity.

Acknowledgements

KLL and JSS are supported by the National Institute of General Medical Sciences of the National Institutes of Health under award number R01GM053275. MES is supported by the Susan G. Komen Career Catalyst Award CCR16380478. JX is supported by the National Science Foundation under grant number DMS-2030355.

Figures & Tables

Parameter	Description	Range/Estimate
β_{11}	child-to-child transmission	$0.05 - 2.0$ per day
β_{12}	child-to-adult transmission	$0.05 - 2.0$ per day
β_{21}	adult-to-child transmission	$0.05 - 2.0$ per day
β_{22}	adult-to-adult transmission	$0.05 - 2.0$ per day
$1/\sigma_1$	child latent period	3 days
$1/\sigma_2$	adult latent period	3 days
$1/\gamma_1$	child infectious period	4 days
$1/\gamma_2$	adult infectious period	4 days
c	multiplier modeling increased child-child contact	10

Table 1: Summary of model parameters with ranges, estimates, and references. The range for transmission between adults is informed by [16]. Latent and infectious period estimates are based on [3, 16].

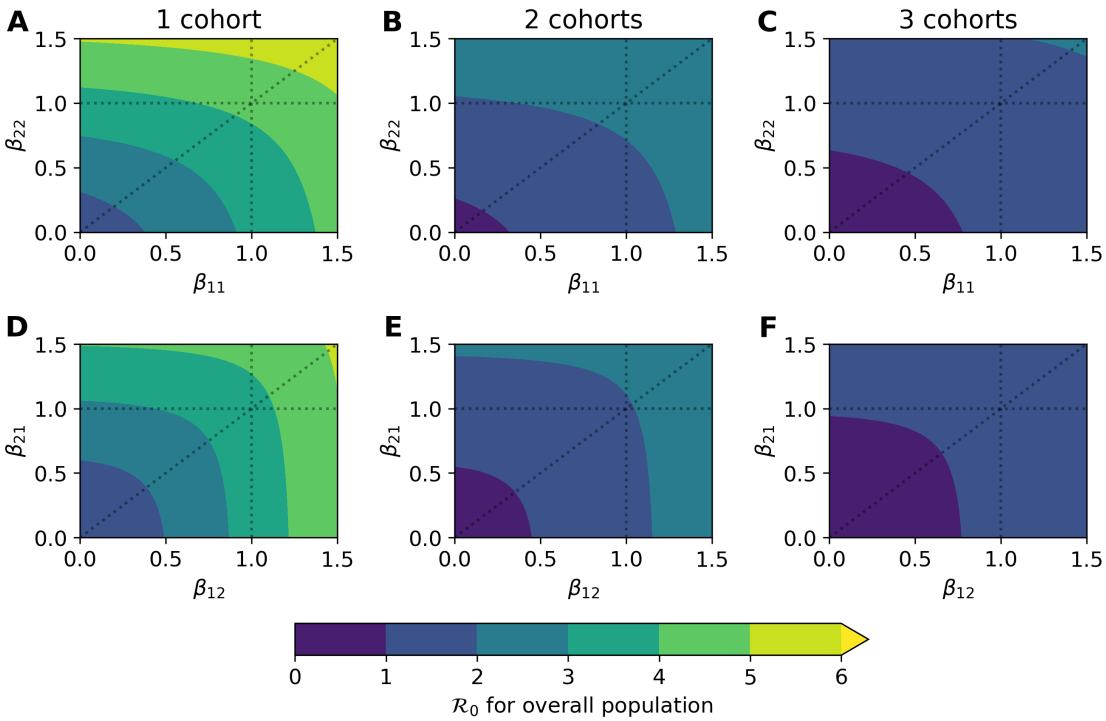

Figure 1: Predicted $\mathcal{R}_0$ under various density and rotating cohort scenarios. Results are based on a latent period of 3 days ($\sigma_1 = \sigma_2 = 1/3$) and an infectious period of 4 days ($\gamma_1 = \gamma_2 = 1/4$). We also assume weak interaction between cohorts ($\alpha_{k\ell} = 0.05$ when $k \neq \ell$). As the color gradient changes from purple to blue, $\mathcal{R}_0$ changes from < 1 to > 1. (A–C) Varying values of β_{11} (child-to-child) and β_{22} (adult-to-adult) rates, assuming transmission between both is equal ($\beta_{12} = \beta_{21} = 0.5$). (D–F) Varying values of β_{12} (child-to-adult) and β_{21} (adult-to-child), assuming transmission within adults is dominant ($\beta_{11} = 0.1$ and $\beta_{22} = 0.5$).

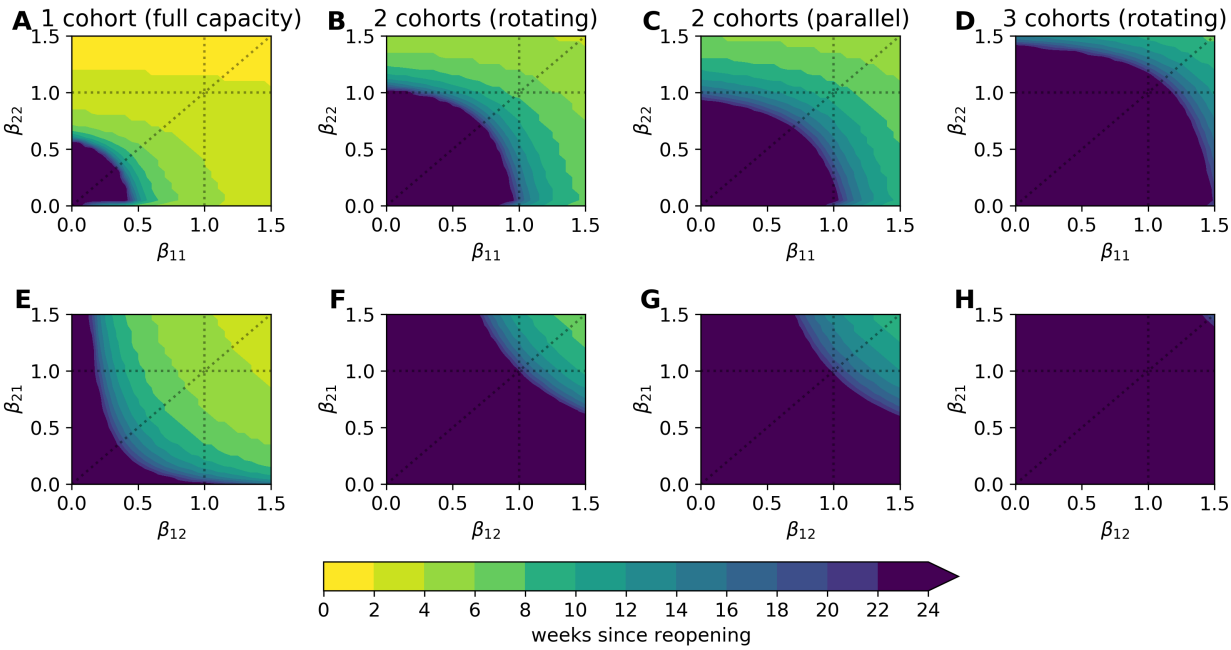

Figure 2: Number of weeks to reach the 5% stopping threshold in a community with equal proportions of adults and children. We use children as representatives of the entire school subpopulation. The 5% threshold tracks cumulative prevalence over all cohorts, $\sum_k [I_{1,k}(t) + R_{1,k}(t)] \geq 0.05 \times \frac{1}{2}$, thus accounting for the size of the schoolchildren population (50%) relative to the overall community. In each simulation, children have an elevated transmission rate due to school contacts over the rate they have when they are not in school; for example, $\beta_{11}(t) = 1 = c \times 0.1$ with $c = 10$. Results are based on latent and infectious periods of 3 and 4 days, respectively ($\sigma_1 = \sigma_2 = 1/3$, $\gamma_1 = \gamma_2 = 1/4$), and the additional assumptions that (A–D) transmission between age classes is equal ($\beta_{12} = \beta_{21} = 0.5$), and (E–H) where adult-to-adult transmission dominates outside of school ($\beta_{11} = 0.1$ and $\beta_{22} = 0.5$). Deep purple is used to indicate scenarios in which the threshold is hit after 22 weeks or more.

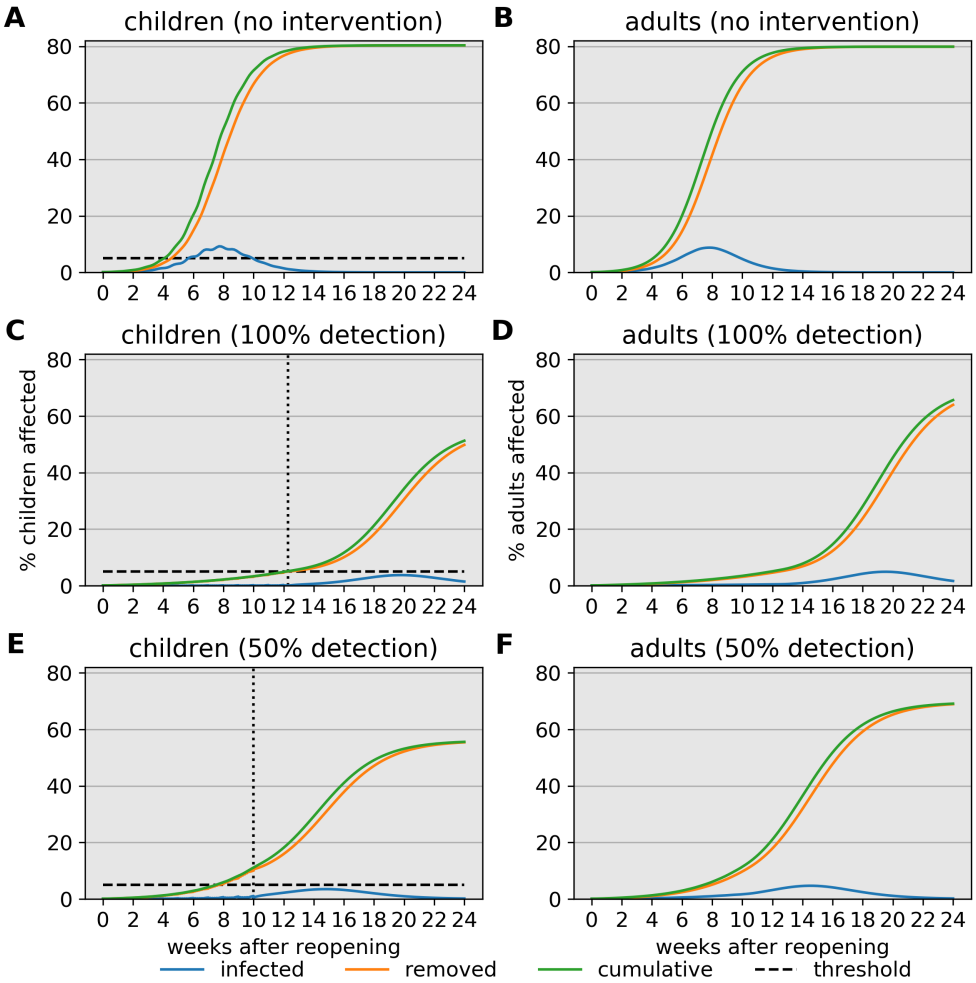

Figure 3: Comparison of outcomes when a school does not track infections (A,B) and when a school reverts to online instruction as a result of a careful screening program (C,D). In both scenarios, the school is assumed to operate at full capacity. Simulations are based on parameter values $\beta_{12} = \beta_{21} = \beta_{22} = 0.5$, $\sigma_1 = \sigma_2 = 1/3$, and $\gamma_1 = \gamma_2 = 1/4$. For child-to-child transmission, we set $\beta_{11}(t) = 0.1$ outside of school and $\beta_{11}(t) = 1 = c \times 0.1$ during school ($c = 10$). Curves correspond to active infections (blue), removed individuals (orange), and cumulative prevalence (green). The school switches to online instruction when detected cases affect 5% of the school population (vertical line), dramatically reducing spread. (E,F) Closures occur earlier and the cumulative prevalence is larger compared to the ideal detection scenario. However, there is not an appreciable increase in long term-infections when the monitoring program has poor detection, and both monitoring scenarios have appreciably less long term infectious than the no intervention scenario.

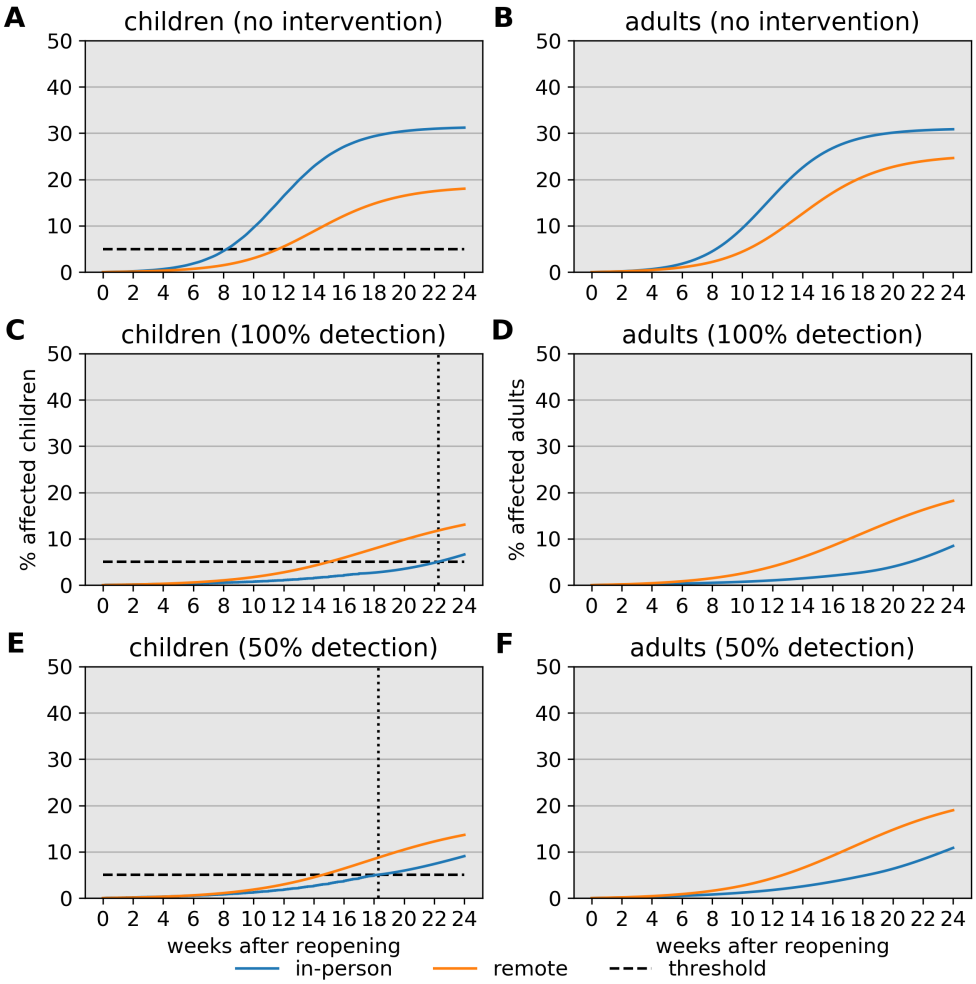

Figure 4: Comparison of cumulative prevalence when half of the school community chooses remote learning (orange) over in-person instruction (blue). Simulations are based on parameter values $\beta_{12} = \beta_{21} = \beta_{22} = 0.75$, $\sigma_1 = \sigma_2 = 1/3$, and $\gamma_1 = \gamma_2 = 1/4$ and assume weak cohort interaction. For child-to-child transmission, we set $\beta_{11}(t) = 0.15$ outside of school and $\beta_{11}(t)1.5 = c \times 0.1$ during school where $c = 10$. Importantly, only one cohort attends school and detection is based on this group. (A,B) Predicted prevalence without any intervention. (C,D) Perfect detection prevents virus spread under modest transmission rates. (E,F) Infections do not increase by a significant amount over a 6 month period when using a less sensitive detection strategy.

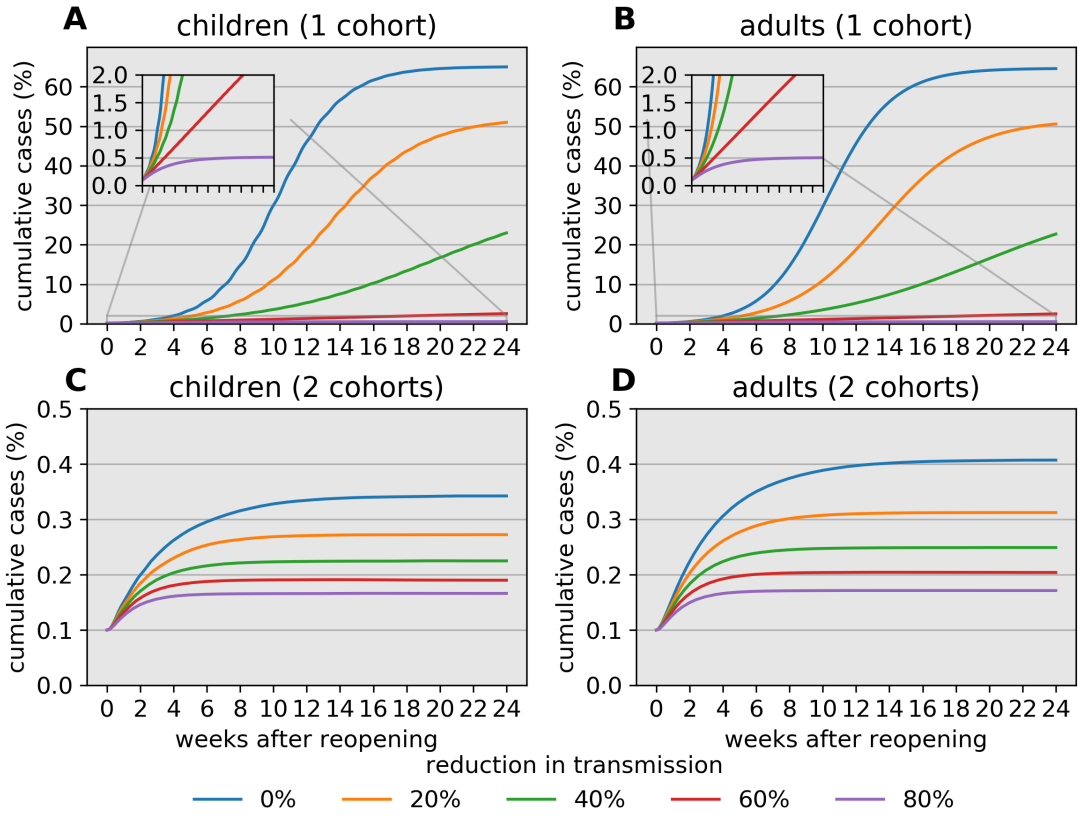

Figure 5: Cumulative prevalence trajectories under risk reduction strategies for children while at school. Simulations are based on parameter values $\beta_{12} = \beta_{21} = \beta_{22} = 0.2$, $\sigma_1 = \sigma_2 = 1/3$, and $\gamma_1 = \gamma_2 = 1/4$, assuming a population with equal numbers of children and adults. For child-child transmission, we set $\beta_{11}(t) = 0.1$ outside of school and $\beta_{11}(t) = (1-r) \times c \times 0.1$ during school, where r is a reduction factor due to effective risk reduction strategies and $c = 10$ accounts for increased contact between children. (A,B) Mitigation that reduces transmission between children can lead to a substantial reduction in infections, provided the mitigation effects are large. (C,D) The impact of risk reduction strategies persists when children are separated into 2 rotating cohorts but does not demand as strict adherence to be effective. An 80% reduction in pediatric transmission is nearly equivalent to separating children into 2 rotating cohorts as both strategies result in fewer than 0.5% pediatric infections over 6 months.

References

[1] Armann, J. P., Unrath, M., Kirsten, C., Lueck, C., Dalpke, A., & Berner, R. (2020). Anti-SARS-CoV-2 IgG antibodies in adolescent students and their teachers in Saxony, Germany (SchoolCoviDD19): Very low seropraevalence and transmission rates. MedRxiv, 2020.07.16.20155143. https://doi.org/10.1101/2020.07.16.20155143

[2] Auger, K. A., Shah, S. S., Richardson, T., Hartley, D., Hall, M., Warniment, A., Timmons, K., Bosse, D., Ferris, S. A., Brady, P. W., Schondelmeyer, A. C., & Thomson, J. E. (2020). Association Between Statewide School Closure and COVID-19 Incidence and Mortality in the US. JAMA. https://doi.org/10.1001/jama.2020.14348

[3] Bar-On, Y. M., Flamholz, A., Phillips, R., & Milo, R. (2020). SARS-CoV-2 (COVID-19) by the numbers. ELife, 9, e57309. https://doi.org/10.7554/eLife.57309

[4] Davies, N. G., Klepac, P., Liu, Y., Prem, K., Jit, M., & Eggo, R. M. (2020). Age-dependent effects in the transmission and control of COVID-19 epidemics. Nature Medicine, 1–7. https://doi.org/10.1038/s41591-020-0962-9

[5] Diekmann, O., Heesterbeek, J. A. P., & Roberts, M. G. (2010). The construction of next-generation matrices for compartmental epidemic models. Journal of The Royal Society Interface, 7(47), 873–885. https://doi.org/10.1098/rsif.2009.0386

[6] Du, Z., Xu, X., Wu, Y., Wang, L., Cowling, B. J., & Meyers, L. A. (n.d.). Serial Interval of COVID-19 among Publicly Reported Confirmed Cases—Volume 26, Number 6—June 2020—Emerging Infectious Diseases journal—CDC. https://doi.org/10.3201/eid2606.200357

[7] He, X., Lau, E. H. Y., Wu, P., Deng, X., Wang, J., Hao, X., Lau, Y. C., Wong, J. Y., Guan, Y., Tan, X., Mo, X., Chen, Y., Liao, B., Chen, W., Hu, F., Zhang, Q., Zhong, M., Wu, Y., Zhao, L., Zhang, F., Cowling, B.J., Li, F., & Leung, G. M. (2020). Temporal dynamics in viral shedding and transmissibility of COVID-19. Nature Medicine, 26(5), 672–675. https://doi.org/10.1038/s41591-020-0869-5

[8] Heald-Sargent, T., Muller, W. J., Zheng, X., Rippe, J., Patel, A. B., & Kociolek, L. K. (2020). Age-Related Differences in Nasopharyngeal Severe Acute Respiratory Syndrome Coronavirus 2 (SARS-CoV-2) Levels in Patients With Mild to Moderate Coronavirus Disease 2019 (COVID-19). JAMA Pediatrics. https://doi.org/10.1001/jamapediatrics.2020.3651

[9] Jones, T. C., Mühlemann, B., Veith, T., Biele, G., Zuchowski, M., Hoffmann, J., Stein, A., Edelmann, A., Corman, V. M., & Drosten, C. (2020). An analysis of SARS-CoV-2 viral load by patient age. MedRxiv, 2020.06.08.20125484. https://doi.org/10.1101/2020.06.08.20125484

[10] Karin, O., Bar-On, Y. M., Milo, T., Katzir, I., Mayo, A., Korem, Y., Dudovich, B., Yashiv, E., Zehavi, A. J., Davidovich, N., Milo, R., & Alon, U. (2020). Adaptive cyclic exit strategies from lockdown to suppress COVID-19 and allow economic activity [Preprint]. Epidemiology. https://doi.org/10.1101/2020.04.04.20053579

[11] Kuhfeld, M., Soland, J., Tarasawa, B., Johnson, A., Ruzek, E., & Liu, J. (2020). Projecting the potential impacts of COVID-19 school closures on academic achievement. In EdWorkingPapers.com. Annenberg Institute at Brown University. https://www.edworkingpapers.com/ai20-226

[12] Kwok, K. O., Lai, F., Wei, W. I., Wong, S. Y. S., & Tang, J. W. T. (2020). Herd immunity – estimating the level required to halt the COVID-19 epidemics in affected countries. Journal of Infection, 80(6), e32–e33. https://doi.org/10.1016/j.jinf.2020.03.027

[13] Larremore, D. B., Wilder, B., Lester, E., Shehata, S., Burke, J. M., Hay, J. A., Tambe, M., Mina, M. J., & Parker, R. (2020). Test sensitivity is secondary to frequency and turnaround time for COVID-19 surveillance. MedRxiv, 2020.06.22.20136309. https://doi.org/10.1101/2020.06.22.20136309

[14] Lauer, S. A., Grantz, K. H., Bi, Q., Jones, F. K., Zheng, Q., Meredith, H. R., Azman, A. S., Reich, N. G., & Lessler, J. (2020). The Incubation Period of Coronavirus Disease 2019 (COVID-19) From Publicly Reported Confirmed Cases: Estimation and Application. Annals of Internal Medicine, 172(9), 577–582. https://doi.org/10.7326/M20-0504

[15] Lee, B., & Raszka, W. V. (2020). COVID-19 Transmission and Children: The Child is Not to Blame. Pediatrics. https://doi.org/10.1542/peds.2020-004879

[16] Li, R., Pei, S., Chen, B., Song, Y., Zhang, T., Yang, W., & Shaman, J. (2020). Substantial undocumented infection facilitates the rapid dissemination of novel coronavirus (SARS-CoV-2). Science, 368(6490), 489–493. https://doi.org/10.1126/science.abb3221

[17] Mitze, T., Kosfeld, R., Rode, J., & Wälde, K. (2020). Face Masks Considerably Reduce COVID-19 Cases in Germany: A Synthetic Control Method Approach. IZA Discussion Paper Series No. 13319. Bonn, Germany: IZA Institute of Labour Economics.

[18] Rackauckas, C., & Nie, Q. (2017). DifferentialEquations.jl – A Performant and Feature-Rich Ecosystem for Solving Differential Equations in Julia. Journal of Open Research Software, 5(1), 15. https://doi.org/10.5334/jors.151

[19] Rackauckas, C., & Nie, Q. (2019). Confederated modular differential equation APIs for accelerated algorithm development and benchmarking. Advances in Engineering Software, 132, 1–6. https://doi.org/10.1016/j.advengsoft.2019.03.009

[20] Seow, J. et al. (2020). Longitudinal evaluation and decline of antibody responses in SARS-CoV-2 infection. MedRxiv, 2020.07.09.20148429. https://doi.org/10.1101/2020.07.09.20148429

[21] Syal, K. (2020). COVID-19: Herd immunity and convalescent plasma transfer therapy. Journal of Medical Virology, 1-3. https://doi.org/10.1002/jmv.25870

[22] Verdoni L, Mazza A, Gervasoni A, et al. An outbreak of severe Kawasaki-like disease at the Italian epicenter of SARS-CoV-2 epidemic: an observational cohort study. Lancet 2020; 395:1771-1778.

[23] Viner, R. M., Russell, S. J., Croker, H., Packer, J., Ward, J., Stansfield, C., Mytton, O., Bonell, C., & Booy, R. (2020). School closure and management practices during coronavirus outbreaks including COVID-19: A rapid systematic review. The Lancet Child & Adolescent Health, 4(5), 397–404. https://doi.org/10.1016/S2352-4642(20)30095-X

[24] Yung, C. F., Kam, K., Nadua, K. D., Chong, C. Y., Tan, N. W. H., Li, J., Lee, K. P., Chan, Y. H., Thoon, K. C., & Ng, K. C. (2020). Novel Coronavirus 2019 Transmission Risk in Educational Settings. Clinical Infectious Diseases. https://doi.org/10.1093/cid/ciaa794

[25] Zhang, J., Litvinova, M., Wang, W., Wang, Y., Deng, X., Chen, X., Li, M., Zheng, W., Yi, L., Chen, X., Wu, Q., Liang, Y., Wang, X., Yang, J., Sun, K., Longini, I. M., Halloran, M. E., Wu, P., Cowling, B. J., Merler, S., Viboud, C., Vespignani, A., Ajelli, M., & Yu, H. (2020). Evolving epidemiology and transmission dynamics of coronavirus disease 2019 outside Hubei province, China: A descriptive and modelling study. The Lancet Infectious Diseases, 20(7), 793–802. https://doi.org/10.1016/S1473-3099(20)30230-9

[26] Zhang, J., Litvinova, M., Liang, Y., Wang, Y., Wang, W., Zhao, S., Wu, Q., Merler, S., Viboud, C., Vespignani, A., Ajelli, M., & Yu, H. (2020). Changes in contact patterns shape the dynamics of the COVID-19 outbreak in China. Science. https://doi.org/10.1126/science.abb8001

[27] Zhu, Y., Bloxham, C. J., Hulme, K. D., Sinclair, J. E., Tong, Z. W. M., Steele, L. E., Noye, E. C., Lu, J., Chew, K. Y., Pickering, J., Gilks, C., Bowen, A. C., & Short, K. R. (2020). Children are unlikely to have been the primary source of household SARS-CoV-2 infections. MedRxiv, 2020.03.26.20044826. https://doi.org/10.1101/2020.03.26.20044826

[28] Zimmerman P, Nigel C. Coronavirus infections in children including COVD-19. The Pediatric Infectious Disease Journal 2020; 39:355-368.

[29] COVID-19 Planning Considerations: Guidance for School Re-entry. (2020, June 25). http://services.aap.org/en/pages/2019-novel-coronavirus-covid-19-infections/clinical-guidance/covid-19-planning-considerations-return-to-in-person-education-in-schools/

[30] Pediatricians, Educators and Superintendents Urge a Safe Return to School This Fall. (2020, July 10). American Federation of Teachers. https://www.aft.org/press-release/pediatricians-educators-and-superintendents-urge-safe-return-school-fall

[31] Governor Gavin Newsom Lays Out Pandemic Plan for Learning and Safe Schools. (2020, July 17). California Governor. https://www.gov.ca.gov/2020/07/17/governor-gavin-newsom-lays-out-pandemic-plan-for-learning-and-safe-schools/

[32] CDC. (2020, August 3). Coronavirus Disease 2019 (COVID-19) in the U.S. Centers for Disease Control and Prevention. https://www.cdc.gov/coronavirus/2019-ncov/cases-updates/cases-in-us.html

[33] DifferentialEquations.jl. SciML. https://github.com/SciML/DifferentialEquations.jl. 07/03/2020. Check-out: v6.15.0.

[34] OrdinaryDiffEq.jl. SciML. https://github.com/SciML/OrdinaryDiffEq.jl. 06/13/2020. Check-out: v5.41.0.